Dual Color Plasmonic Pixels Create a Polarization Controlled Nano Color Palette

Zhibo Li, Alasdair W. Clark*, Jonathan M. Cooper

Biomedical Engineering Research Division, School of Engineering, Rankine Building, University of Glasgow, Glasgow, G12 8LT

Email: alasdair.clark@glasgow.ac.uk, Tel: 0141 330 3216

Abstract

Color filters based upon nano-structured metals have garnered significant interest in recent years, having been positioned as alternatives to the organic dye-based filters which provide color selectivity in image sensors, as non-fading 'printing' technologies for producing images with nanometer pixel resolution, and as ultra-high-resolution, small foot-print optical storage and encoding solutions. Here, we demonstrate a plasmonic filter set with polarization-switchable color properties, based upon arrays of asymmetric cross-shaped nano-apertures in an aluminum thin-film. Acting as individual color-emitting nano-pixels, the plasmonic cavity-apertures have dual-color selectivity, transmitting one of two visible colors, controlled by the polarization of the white light incident on the rear of the pixel and tuned by varying the critical dimensions of the geometry and periodicity of the array. This structural approach to switchable optical filtering enables a single nano-aperture to encode two information states within the same physical nano-aperture; an attribute we use here to create micro image displays containing duality in their optical information states.

Keywords: nanoplasmonics, metasurfaces, color printing, plasmonic pixels, color filter, nano cavity apertures, nano holes.

A trait that nearly all imaging and display technologies share is the requirement to selectively project or collect light of different wavelengths; breaking white-light down into component parts (typically red, green and blue) for color image recording or projection. This separation is

achieved through the inclusion of various filters, which in most commercial applications are based on absorption *via* organic dyes; facilitating the need for relatively thick polymer materials with long optical paths that are not conducive to high pixel densities, and are also prone to environmental damage and degradation. As an alternative to these strategies, inorganic nano-scale filters based on engineered metal nanostructures are becoming increasingly appealing.[1 2, 3] Structural nano-filters separate light due to the engineered plasmon resonances of their constituent nanostructures. Determining which wavelengths of light are absorbed, scattered or transmitted, the resonant characteristics of a particular structure can be tuned by altering its geometry and composition.[4] Unlike conventional dye-doped polymers, these plasmonic filters can perform over length scales of <100 nm, making them particularly relevant to ultra-high resolution imaging applications, where the absorption limitations and fabrication challenges surrounding conventional filter miniaturization are proving to be a significant technical hurdle in delivering the next generation of image capture and display technologies.[1, 5]

Although in their infancy, plasmonic filters consisting of positive nanostructures have already been demonstrated as successful for full-color light separation in both transmissive and reflective systems,[3, 6-10] and have enabled colour image reproduction and display at the micro-scale; producing images with a 'printed' resolution that extends beyond the diffraction limit, and far exceeds the resolution limit of current color-printing technologies.[2, 3] They have also been employed in optical storage technologies,[11] as a means to produce ultra-high resolution stereoscopic images,[9] incorporated with active media to enable a degree of color tunability,[12] and exploited as color reporters for biosensor applications.[13] As an alternative to filters constructed using positive nanostructures, plasmonic filters comprised of 'negative' structures are also effective for separating white light. Comprised of nano-scale apertures penetrating a metallic thin-film, plasmonic cavity-apertures are typically simpler to produce than their positive counterparts, and provide a less fabrication intensive route towards color selectivity.[1, 14, 15]

Furthermore, these arrangements are perfectly suited to integration with existing CMOS image sensor technologies, such that full-color images can be obtained.[16, 17]

The implementation of these cavity-aperture filters is underpinned by the phenomena of extraordinary optical transmission (EOT) through periodic sub-wavelength apertures patterned in an otherwise optically opaque aluminum film.[18] At normal light incidence, the nano-apertures act as grating couplers, providing photon-plasmon momentum matching to allow surface plasmon resonances (SPR) at the metal/dielectric interface. It is already well established that in such circumstances the plasmon tunnels through the aperture and decays to radiant photons upon penetrating the metal film.[19-24] By varying the size, shape, thickness and periodicity of the array, it is known that the permitted plasmon coupling frequency can be tuned, dictating the color of the transmitted light.[15, 17, 25, 26]

Typically, plasmonic cavity-aperture filters are comprised of circular nano-holes tuned to operate efficiently at a single wavelength.[27] However, in filtering applications such as polarimetry microscopy, security encryption and hyperspectral imaging, often dual or multi-color filtering is necessary, a requirement currently enabled by increasing the number of different filtering elements.[28-30] In this paper, we explore dual-color transmissive plasmonic nano-pixels, designed to encode more than a single wavelength, with color selectivity provided by controlling the polarization of the white light incident on the rear of the pixel. Using asymmetric, cross-shaped apertures, we show that a single aperture can support two, independently tunable color transmission modes in the visible spectrum. Using these dual-color nano-pixels, we demonstrate a polarization sensitive color palette that can be employed to create complex images with dual information states at resolutions far beyond the diffraction limit. These pixels hold the potential to improve upon current plasmonic pixel technology by enabling smaller, more versatile filter sets for nano-scale imaging and storage applications, where, significantly, a

single array can function at two selectable filtering regimes within the same unit area, allowing optical storage of 2 information layers using the same dual-action pixels.

The operation of these pixels relies upon the selection rules for free-space propagating light encountering a slit; rules which determine the wavelengths transmitted as a function of the size, shape and orientation of the slit, as well as the periodicity of the arrayed apertures. Paramount among these rules is the requirement for the transverse electric-field component of the incident light to be perpendicular to the length of the slit; a condition without which no light will be permitted through the aperture, regardless of wavelength.[31] Our pixels comprise asymmetric, cross-shaped apertures (acting as intersecting slits aligned perpendicular to one another) in a 100 nm aluminum thin-film, capped with 150 nm of SiO_2. Aluminum's high plasmon frequency allows visible wavelength transmission with a lower optical loss than gold and silver alternatives,[6, 7, 10, 32] with the added advantage of being abundant, low cost, and fully compatible with current industrial CMOS fabrication processes.

Results and Discussion

Figure 1 shows schematics of an isolated asymmetric nano-pixel, 4 pixels in an array configuration, and an SEM of a typical fabricated pixel array. A number of different asymmetric cross configurations were fabricated, each having a long 'arm' and a short 'arm', which will be referred to as LA and SA respectively from this point onwards. In all cases the slit width (the width of the each arm) was fixed at 30 +/- 2 nm and the thickness of the aluminum film was fixed at 100 nm.

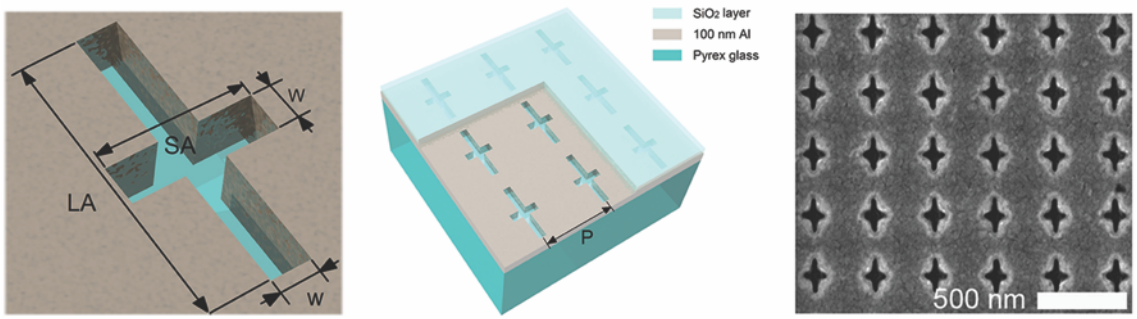

Figure 1. Schematics and SEM showing aperture geometry and arrangement. All errors stated represent standard deviation. Schematics (left and middle): LA and SA refer to the long arm and short arm respectively, P and w refer to the array periodicity and arm slit width respectively. SEM (right): Large area image of a typical pixel array. Average aperture dimensions are, LA= 203 +/- 3 nm, SA= 120 +/- 5 nm, P=340 nm, and w= 30 +/- 2 nm (the width of each arm is identical).

To test this methodology for generating dual-color pixels, palettes containing 16 pixel arrays (numbered 1-16) were fabricated as a 100×100 μm squares containing different pixel geometries. **Figure 2** shows bright-field transmission images of this test palette when the electric-field of white-light incident on the rear of the palette was polarized along the SA and LA axis of the apertures for **2a** and **2b** respectively (a linear polarizer was used to control the polarization of the light). In each case, the LA length was measured as 203 +/- 3 nm, while the SA lengths were varied from 120 nm to 180 nm in 20 nm increments, moving top to bottom in **Figure 2** (average measurements from 20 examples of each pixel revealed these SA lengths to be 120 +/- 5 nm, 140 +/- 5 nm, 158 +/- 4 nm, and 179 +/- 5 nm). The periodicity of apertures within each array was also varied, from 250 nm to 340 nm in 30 nm increments (moving left to right in **Figure 2**).

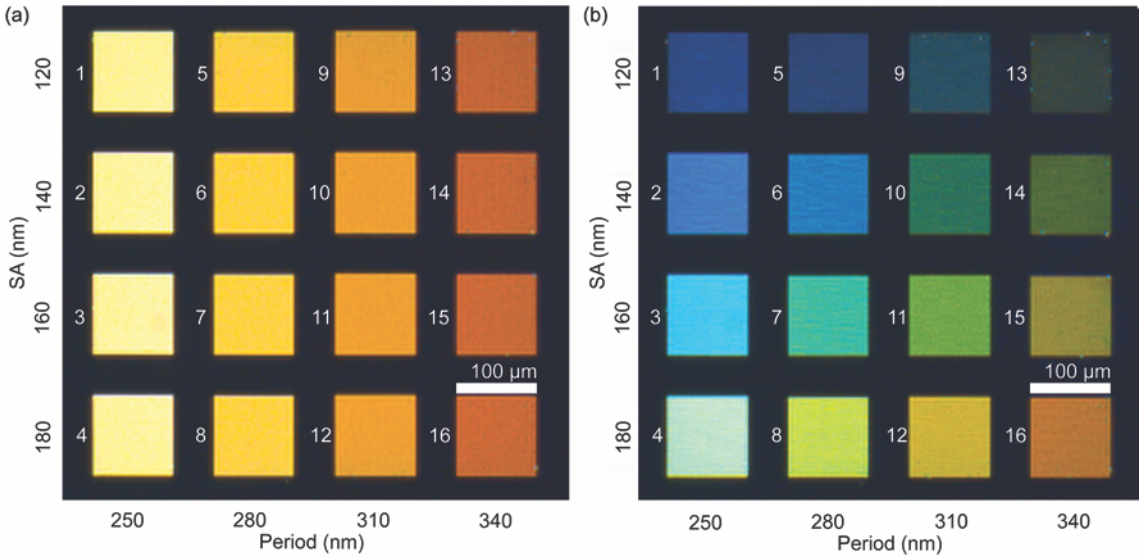

Figure 2. Polarization switchable color palette. Bright-field microscope images of the nano-pixels back-illuminated with a white-light source. **a.** Shows the transmitted color when the light is polarized along the x-axis short arm (resulting in transmission through the long arm); **b.** Shows the transmitted color when the light is polarized along the y-axis long arm (resulting in transmission through the short arm). The drop in intensity seen as the period increases is due to there being less apertures per unit area.

Only 4 colors are apparent in **Fig. 2(a)** since the LA length for each array is identical (203 +/- 3 nm). The color difference seen from column to column in this polarization state results solely from a change in array periodicity. **Figure 2(b)** shows the color when the light is transmitted through the shorter arm of the pixel (the electric-field polarized perpendicular to the short arm). Since both the short-arm length and the pixel periodicity are different for each of the 16 arrays, there is a gradual red-shift in transmitted colors from high frequency blue wavelengths at the shortest arm length and smallest period, to low-frequency reds at the longest arm length and largest periods. Significantly, there is a distinct difference between the colors transmitted by the long and short-arms of the same pixel array, showing that a single geometry can be tuned to selectively produce two colors in the visible spectrum (In the case of a symmetric cross, with equal arm lengths in x and y, the colors produced at each polarization would be identical). As a

direct consequence of the polarization dependant transmission requirements, the resonance of one arm does not effect that of the other, giving full tunability between modes, with the color resolution is limited only by the resolution of the fabrication process.

Figure 3 shows the transmission spectra associated with each of the 16 fabricated arrays, measured at both polarization states. The spectra show that the plasmonic response from each pixel's LA transmission varies only a small amount between pixels with the same period (pixels 1-4 in **(a)i,** for example), hence the indistinguishable colors these pixels produce in **Figure 2**. Increasing the period of the features from 250 nm to 340 nm (in 30 nm increments from **(a)i.** to **(a)iv**.) shifts the peak transmission wavelength from 646 nm to 659 nm (average peak values from each set of 4 pixels). The geometry and the period of a given array do not, however, by themselves account for the change in transmitted color. In the two sets of pixels, 1-4 and 13-16 in **Figure 2**, the actual transmitted colors (off-white and red, respectively) are not as a consequence of the peak transmission wavelengths alone, but are also impacted by the sharpness of the resonance, which increases with the expansion in array period; the average FWHM drops from 360 nm for a period of 250 nm, to 120 nm for a period of 340 nm (when comparing pixels 1-4 with pixels 13-16, **Figure S1(a),** Supporting Information). Increasing the period of the array therefore narrows the spectral range of the permitted SPR coupling energies, resulting in more distinct colors which appear closer to the wavelength of the peak value (which we see as a transition from off-white, through two shades of yellow/orange, to red as the FWHM is decreased and the color contributions from wavelengths surrounding the peak wavelength are narrowed, **Figure 2(a)**, columns, from left to right [plotted in **Figure S1(b),** Supporting Information]). Predictably, the larger period also manifests itself as a drop in transmitted light intensity (from a peak of 12% to <5%), as there are fewer apertures per unit area through which the light can propagate.

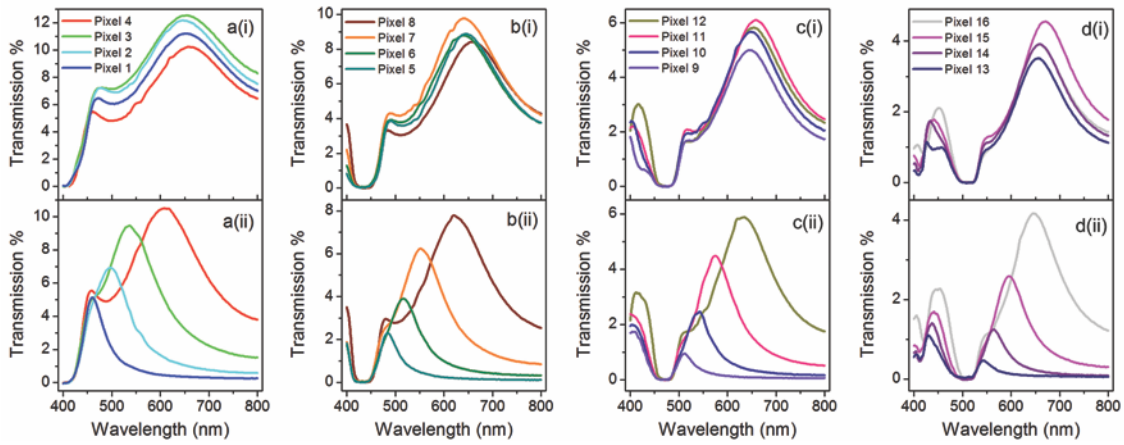

Figure 3. Experimentally measured optical transmission spectra of each pixel variant. For ease of reading, the spectra have been grouped according to their period. **a(i) and a(ii),** Pixels 1-4, transmission through the LA and SA arms respectively. **b(i) and b(ii),** Pixels 5-8, transmission through the LA and SA arms respectively. **c(i) and c(ii),** Pixels 9-12, transmission through the LA and SA arms respectively. **d(i) and d(ii),** Pixels 13-16, transmission through the LA and SA arms respectively.

Although it is possible to tune color transmission through manipulation of the periodicity alone, a more effective method is to also alter the length of the arms. **Figure 3 (a)ii, (b)ii, (c)ii** and **(d)ii**, show the transmitted wavelengths for pixels 1-16 when light is transmitted through the short arm of each pixel. Within each sub-set of 4 pixels the period was the same, but the length of the arm was increased from 120 nm to 180 nm in 20 nm increments. The effect of this 60 nm increase is a significant red-shift in the transmission peak; shifting by 148 nm, 140 nm, 123 nm and 104 nm for **(a)ii, (b)ii, (c)ii and (d)ii** respectively (plotted in **Figure S2(a)**, Supporting Information). We also see an increase in transmission as the arm length increases; as the aperture becomes larger, it can transmit more light. As was the case for the LA transmission, here we also observe a FWHM narrowing and a peak red-shift due to an increase in array periodicity (plotted in **Figure S2(b)** and **(c)**, Supporting Information). Comparing the SA transmission of pixel 3 with pixel 15 (identical geometries with periodicities of 250 nm and 340

nm respectively) sees a red-shift, based purely on periodicity, of 59 nm. Since the distance between the tips of the long arms determines the SA transmission curve, and vice versa,[31] we see a larger shift in SA transmission relative to LA transmission with increasing period. The 90 nm period increase, from pixels 1-4 to 13-16, results in the tip-to-tip distance increasing by 2.8x for the fixed-length long arms, and by 1.7x, 1.8x, 2x and 2.3x for the varying-length short arm pixels (relating to pixels 1-4, 5-8, 9-12 and 13-16 respectively). As with the LA transmission, for fixed periods we also see spectral narrowing with increased period, and in addition to this, we see significant spectral narrowing as the length of the arm is decreased (the 60 nm drop in SA length leads to FWHM drops of 167 nm, 159 nm, 144 nm and 110 nm for pixels 1-4, 5-8, 9-12 and 13-16 respectively, plotted in **Figure S2(d)**, Supporting Information).

As **Figures 2**, **3, S1** and **S2** demonstrate, in order to achieve a particular range of color output for these filters, a balance must be struck between aperture size and periodicity. Although spectrally narrow features are desirable, achieving them, by increasing the array period, sacrifices high-frequency transmission (blues) and leads to a decrease in the transmission efficiency. In a similar trade-off, larger features (longer arm lengths) would lead to a greater transmission efficiency, but at the detriment of spectral width and, once again, high-frequency transmission. Given the geometric constraints placed on the pixel periodicity and arm length required to keep the transmission in the visible range, and prevent the pixels overlapping with one another, there is little latitude left for tuning *via* these factors alone. However, another tuning option available in this system is the thickness of the aluminum film the apertures are pattern in. Increasing the thickness of the film to 125 nm leads to a spectral narrowing of the transmission for each pixel variant, and a significant blue-shift in the transmission spectra which made low-frequency colors (red) difficult to access. In contrast, decreasing the film thickness to 75 nm led opposite issues; a significant spectral broadening of each peak, and a red-shifted response which made high-frequency blues inaccessible (**Figures S3** and **S4** in Supporting

Information show the transmission characteristics of pixels 1-16 for film thicknesses of 75 nm and 125 nm compared to the 100 nm data shown above, as well as CIE1931 plots showing the color range of these pixels for each film thickness). As a result, the Al film thickness chosen for the main study was 100 nm (**Figures 2** and **3**), as this presented the best compromise for maintaining a color palette with access to the full visible spectrum. No difference in transmission efficiency was seen across this thickness range for the pixel geometries investigated.

The electric-field distribution of the individual pixels was calculated using a FDTD simulation. **Figure 4** contains a representative example of these simulations for a geometry identical to pixel 6 (140 +/- 5 nm x 203 +/- 3 nm with a period of 280 nm); showing the measured and simulated transmission spectra, as well as the electric field distribution at the entrance, centre and exit of the aperture, at peak resonance wavelength, for both polarization states. The simulated transmission spectra in **Figure 4 (a)i** and **(b)i** show good agreement with the experimental results. The localised electric-field within the void **(Figure 4 (a) & (b) ii-iv)**, varies in intensity as the plasmon propagates through the aperture. For both polarizations, the fields are strongest at the entrance and exit of the aperture (in this case with enhancements of 190x and 210x the incident field for the LA and SA respectively), and weakest in the centre of the aperture (where the maximum enhancement is 55x and 47x the incident field for the LA and SA respectively).

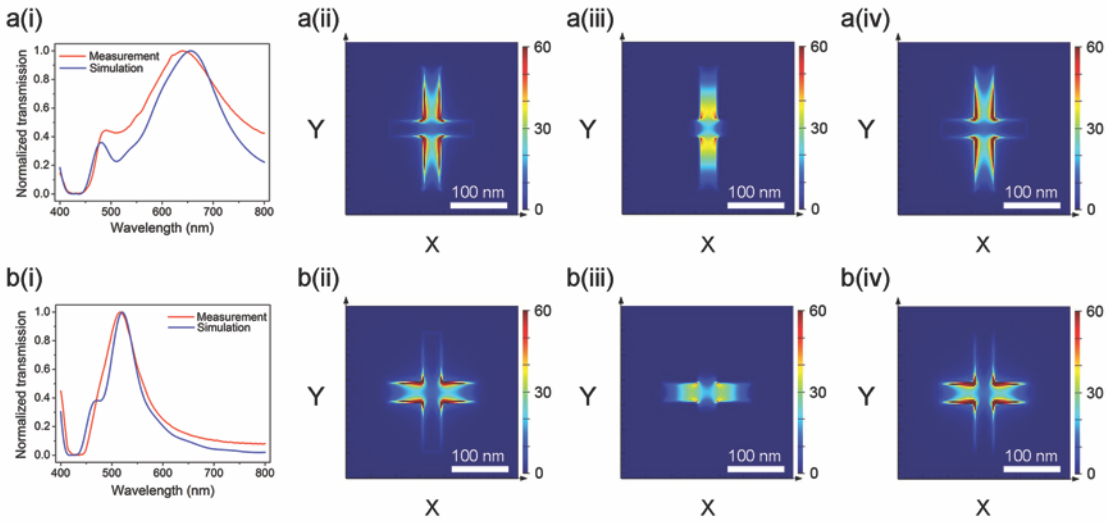

Figure 4. Numerical simulations of the plasmonic response of Pixel 6. **a(i)** and **b(i),** Experimental and simulated transmission spectra through the LA and SA respectively. **a(ii-iv)** and **b(ii-iv)**, Resonant electric-field distributions at LA and SA transmission (**a** and **b** respectively) at 0 nm, 50 nm and 100 nm through the Al thin-film (**ii, iii** and **iv** respectively). The experimental data matches the simulated data well. The small differences seen are likely due to slight fabrication variance between each aperture in the large array, something the simulation does not take into account.

Since each pixel acts as an individual color emitter, it is possible to further tune the transmission of the filters by creating arrays comprised of multiple pixel geometries in different ratios (***i.e.*** color mixing). **Figure 5** shows how different colors can be generated by combining different ratios of 'blue' and 'yellow' pixels, in this case the short-arm transmission of pixels 5 and 8. As both the bright-field images and the transmission spectra of these arrays show, taking a fully 'blue' array and increasing its proportion of yellow pixels results in the transmitted color, as perceived in the far-field, to shift through a gradient of distinct colors as the contribution from the blue transmission peak decreases and the yellow transmission peak increases.

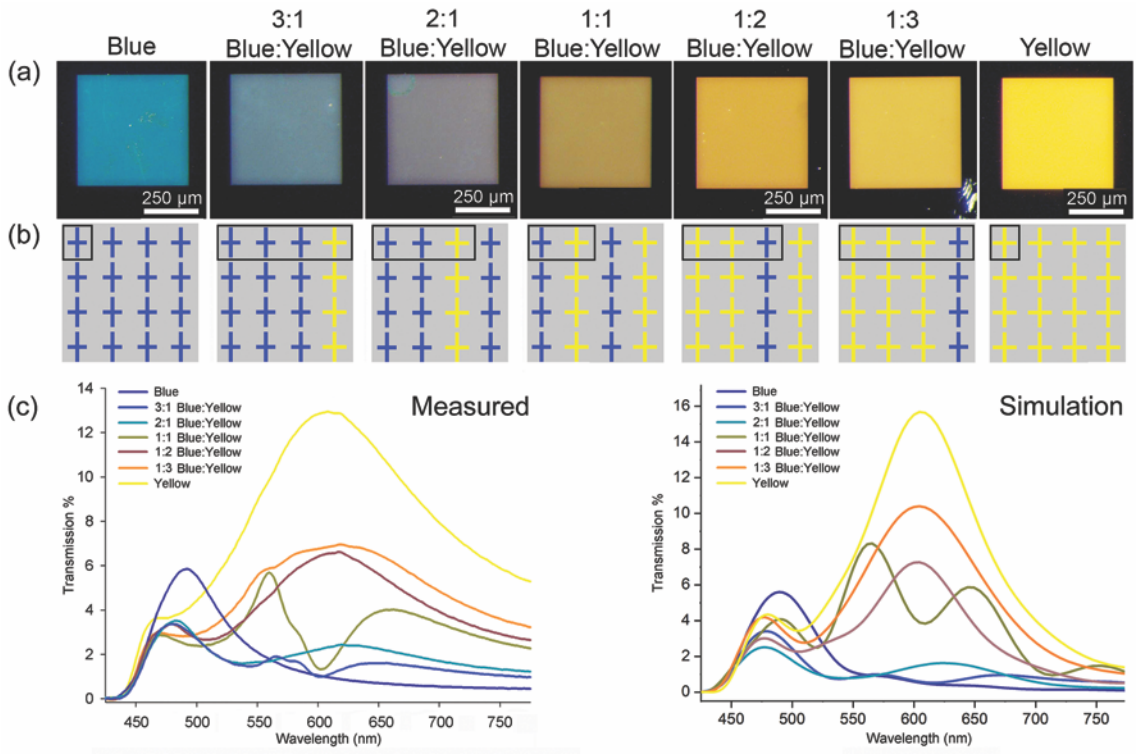

Figure 5. Varying the ratio of different pixel types within an array to perform color-mixing**. (a)** Bright-field microscope images of 7 color pixel arrays with different ratios of pixel 5 (blue) and pixel 8 (yellow). **(b)** Schematic representations of each pixel ratio. The pixels contained within the black box represent the repeating pattern which makes up each array. **(c)** Measured and simulated transmission spectra for each array. In all cases the electric field was polarized such that light is propagating through the short-arm of the pixels. Arrays with a higher proportion of 'yellow' pixels display higher transmission values due to these apertures being significantly larger than their blue counterparts (180 nm for yellow, 120 nm for blue). The larger the aperture, the more light is transmitted. The calculated and measured spectra are in good agreement.

A major driver of recent research into sub-wavelength plasmonic color pixels has been their potential for utilisation as new filtering elements for display and imaging technologies,[12, 16, 33, 34] ultra-high resolution 'printing',[2, 3] and optical data storage.[11] In order to demonstrate the potential of our dual-color pixels in these areas, we have used them to generate microscopic images that display different color information states when illuminated with different light

polarizations. **Figure 6 (b** & **c)** show two microscopic University of Glasgow logos with switchable outputs. Logo 1 (**Figure 6(b)**) consists of a single pixel geometry (Pixel 1) that has been patterned in two orientations; the long arm orientated along the x-axis for the background and along the y-axis for the lettering (an SEM showing the detail of this arrangement can be seen in **Figure 6(a)**). The result of this arrangement is that when the electric-field component of the white-light incident on the rear of the logo is changed from oscillating along the x-axis (**Figure 6(b)i**) to oscillating along the y-axis (**Figure 6(b)ii**), the color of the background and the lettering flip.

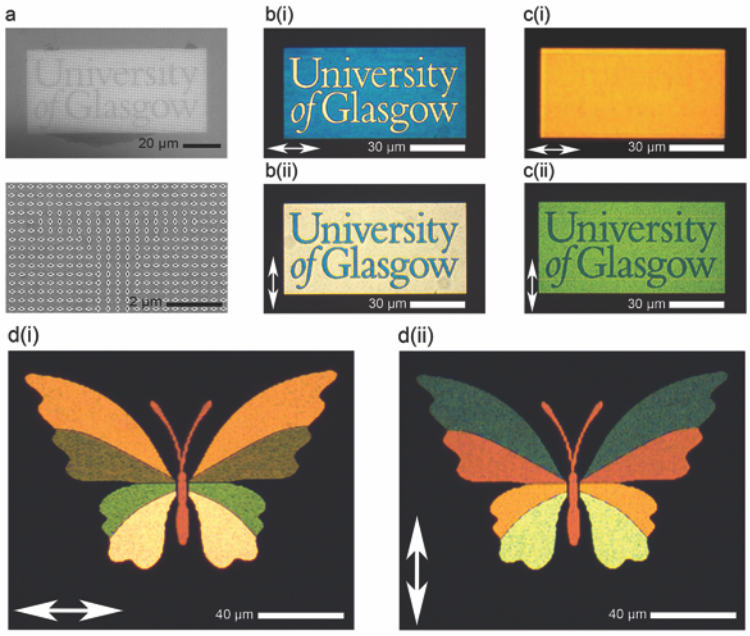

Figure 6. Microscopic images with dual color information states 'printed' with nano-scale resolution. All errors stated represent standard deviation. **a.** A SEM image of logo1, with enlarged view shows the top right part of letter U. Pixel 1 (LA= 203 +/- 3 nm, SA= 120 +/- 5 nm and P= 250 nm) was used for making logo pattern 1, the pixels in letter sections are rotated through 90 degrees with respect to those in the background region. **b(i)** Optical transmission image of logo 1 with the incident electrical field along the x-axis. **b(ii)** Optical transmission image of logo 1 with the incident electrical field along the y-axis. **c(i)** Optical transmission image of logo 2 with incident electrical field along the x-axis. **c(ii)** Optical transmission image of logo 2

with incident electrical field along the y-axis. Pixel 9 and pixel 10 were used in the letter and background regions, respectively. Both pixels had the same LA (203 +/- 3 nm) and P (310 nm), but the SA was 120 +/- 5 nm in pixel 9 and 140 +/- 5 nm in pixel 10. **d(i) & (ii)** Microscopic images of a butterfly with switchable wing panel colors due to the electric-field of the incident light being polarized along the x and y-axes respectively (the arrows display the oscillation direction of the electric-field).

As well as encoding images with two color states, images which display different information at different polarizations can also be created. In Logo2 (**Figure 6(c) i** and **ii**) we use two different geometries of pixel (Pixels 9 and 10), rather than the single geometry that was used in Logo1. For Logo2, the background comprised Pixel 10 and the lettering of Pixel 9. Both sets of pixel arrays were arranged in the same orientation (the long arm parallel to the y-axis of **Figure 6)).** The pixel dimensions that were chosen so that the color they produce when the plasmon propagates through their long-arm is identical, whereas the colors produced when light propagates through their short-arm is different. As can be seen from the transmitted images in **Figure 6(c)i and ii**, this results in an orange rectangle at one polarization and a full green and blue University of Glasgow logo at the opposite polarization. Further examples of the potential for dual-color image printing can be seen in **Figures 6 (d)**, where we show that this technique can be used to create images with switchable color schemes at extreme resolutions.

Conclusion

In summary, we have demonstrated a versatile transmissive filter set comprised of single-geometry, dual-color nano-pixels, fabricated as cross-shaped plasmonic cavity-apertures in an aluminum thin-film. The single geometry pixels exhibit two distinct, polarization-dependent resonances, which can be tuned across the visible spectrum by altering the geometry of the aperture and the periodicity of the array. Significantly, this allows the pixels to be patterned in

such a way as to create images with nano-scale feature resolution, and encoded with dual color and information states, switched by controlling polarization of the incident white-light. As a result, cavity-aperture pixels of this type could impact future display, printing, high-density optical data storage, imaging and filtering technologies.

Methods

Pixel fabrication: The nano-pixel arrays were fabricated using electron-beam lithography, reactive ion etching (RIE), and inductively coupled plasma (ICP) deposition. Each array was fabricated on a 500 μm Pyrex glass substrate which had been modified with a 100 nm aluminum thin-film, deposited by electron beam evaporation. A 200 nm layer of ZEP520A was spin coated onto the aluminum and subsequently patterned using a Vistec VB6 UHR EWF electron beam lithography tool. After resist development, the exposed aluminum patterns were etched using $SiCl_4$ gas in an Oxford Instrument System 100 RIE tool. The remaining resist was then stripped before a 150 nm SiO_2 layer was deposited, using a Oxford Instrument System 100 ICP deposition tool. The SiO_2 cap layer deposited on top of the metallic structure enhances the optical transmission through the apertures, albeit at the expense of a red-shift to the resonance wavelength which must be compensated for in the design stage. [35]

Optical characterisation: Optical transmission images of the pixel arrays and the chromatic patterns were captured using a CCD camera and a Zeiss Axio Imager A1 optical microscope with a 50x 0.5NA objective. Transmission spectra of the pixel arrays were measured using a Shimadzu UV3101PC spectrophotometer with a linear film polariser. The measured wavelength range was 400 to 800 nm.

Numerical characterisation: Simulations of the plasmonic transmission spectra and resonant electric-field distribution were performed using Lumerical finite-difference-time-domain (FDTD)

software (7.5.2). The minimum meshing element size was 3 nm. A perfectly matched layer was set in the top and bottom Z planes to prevent unwanted reflections, while periodic boundary conditions were applied to the X and Y planes, enabling the single unit simulation to represent the behaviour of an infinite array. The dielectric functions of aluminum and SiO_2 were set to Palik's values[36] for all the calculations.

Acknowledgements

This work was supported by Royal Academy of Engineering (grant number 10216/103). The authors also wish to acknowledge China Scholarship Council (CSC) and the ERC Advanced Grant, Bio-Phononics (340117) for supporting this work. The authors also thank all the staff working in the James Watt Nanofabrication Centre (JWNC) at the University of Glasgow for their support.

Supporting Information Available: Supporting Information includes peak and FWHM tuning data for each pixel as a result of geometry and periodicity changes; transmission spectra and related tuning data for different Al film thicknesses; and plots of the CIE1931 chromaticity coordinates for the pixels produced using different Al thickness. This material is available free of charge via the Internet at http://pubs.acs.org.

References

1. Gu, Y.; Zhang, L.; Yang, J. K. W.; Yeo, S. P.; Qiu, C.-W. Color Generation Via Subwavelength Plasmonic Nanostructures. *Nanoscale* **2015**, 7, 6409-6419.

2. Kumar, K.; Duan, H.; Hegde, R. S.; Koh, S. C. W.; Wei, J. N.; Yang, J. K. W. Printing Colour at the Optical Diffraction Limit. *Nat. Nanotechnol.* **2012**, 7, 557-561.

3. Tan, S. J.; Zhang, L.; Zhu, D.; Goh, X. M.; Wang, Y. M.; Kumar, K.; Qiu, C.-W.; Yang, J. K. W. Plasmonic Color Palettes for Photorealistic Printing with Aluminum Nanostructures. *Nano Lett.* **2014**, 14, 4023-4029.

4. Hutter, E.; Fendler, J. H. Exploitation of Localized Surface Plasmon Resonance. *Adv. Mater.* **2004**, 16, 1685-1706.

5. Dean, N. Colouring at the Nanoscale. *Nat. Nanotechnol.* **2015**, 10, 15-16.

6. Shrestha, V. R.; Lee, S.-S.; Kim, E.-S.; Choi, D.-Y. Aluminum Plasmonics Based Highly Transmissive Polarization-Independent Subtractive Color Filters Exploiting a Nanopatch Array. *Nano Lett.* **2014**, 14, 6672-6678.

7. Ellenbogen, T.; Seo, K.; Crozier, K. B. Chromatic Plasmonic Polarizers for Active Visible Color Filtering and Polarimetry. *Nano Lett.* **2012**, 12, 1026-1031.

8. Roberts, A. S.; Pors, A.; Albrektsen, O.; Bozhevolnyi, S. I. Subwavelength Plasmonic Color Printing Protected for Ambient Use. *Nano Lett.* **2014**, 14, 783-787.

9. Goh, X. M.; Zheng, Y. H.; Tan, S. J.; Zhang, L.; Kumar, K.; Qiu, C. W.; Yang, J. K. W. Three-Dimensional Plasmonic Stereoscopic Prints in Full Colour. *Nat. Commun.* **2014**, 5, 5361.

10. Olson, J.; Manjavacas, A.; Liu, L.; Chang, W.-S.; Foerster, B.; King, N. S.; Knight, M. W.; Nordlander, P.; Halas, N. J.; Link, S. Vivid, Full-Color Aluminum Plasmonic Pixels. *Proc. Natl. Acad. Sci. U. S. A.* **2014**, 111, 14348-14353.

11. Zijlstra, P.; Chon, J. W. M.; Gu, M. Five-Dimensional Optical Recording Mediated by Surface Plasmons in Gold Nanorods. *Nature* **2009**, 459, 410-413.

12. Franklin, D.; Chen, Y.; Vazquez-Guardado, A.; Modak, S.; Boroumand, J.; Xu, D.; Wu, S.-T.; Chanda, D. Polarization-Independent Actively Tunable Colour Generation on Imprinted Plasmonic Surfaces. *Nat. commun.* **2015**, 6, 7337.

13. Clark, A. W.; Cooper, J. M. Plasmon Shaping by Using Protein Nanoarrays and Molecular Lithography to Engineer Structural Color. *Angew. Chem., Int. Ed.* **2012**, 51, 3562-3566.

14. Chen, Q.; Cumming, D. R. S. High Transmission and Low Color Cross-Talk Plasmonic Color Filters Using Triangular-Lattice Hole Arrays in Aluminum Films. *Opt. Express* **2010**, 18, 14056-14062.

15. Inoue, D.; Miura, A.; Nomura, T.; Fujikawa, H.; Sato, K.; Ikeda, N.; Tsuya, D.; Sugimoto, Y.; Koide, Y. Polarization Independent Visible Color Filter Comprising an Aluminum Film with Surface-Plasmon Enhanced Transmission through a Subwavelength Array of Holes. *Appl. Phys. Lett.* **2011**, 98, 093113.

16. Burgos, S. P.; Yokogawa, S.; Atwater, H. A. Color Imaging Via Nearest Neighbor Hole Coupling in Plasmonic Color Filters Integrated onto a Complementary Metal-Oxide Semiconductor Image Sensor. *Acs Nano* **2013**, 7, 10038-10047.

17. Yokogawa, S.; Burgos, S. P.; Atwater, H. A. Plasmonic Color Filters for Cmos Image Sensor Applications. *Nano Lett.* **2012**, 12, 4349-4354.

18. Ebbesen, T. W.; Lezec, H. J.; Ghaemi, H. F.; Thio, T.; Wolff, P. A. Extraordinary Optical Transmission through Sub-Wavelength Hole Arrays. *Nature* **1998**, 391, 667-669.

19. Pendry, J. B.; Martín-Moreno, L.; Garcia-Vidal, F. J. Mimicking Surface Plasmons with Structured Surfaces. *Science* **2004**, 305, 847-848.

20. Brolo, A. G.; Kwok, S. C.; Moffitt, M. G.; Gordon, R.; Riordon, J.; Kavanagh, K. L. Enhanced Fluorescence from Arrays of Nanoholes in a Gold Film. *J. Am. Chem. Soc*. **2005**, 127, 14936-14941.

21. Dintinger, J.; Klein, S.; Ebbesen, T. W. Molecule–Surface Plasmon Interactions in Hole Arrays: Enhanced Absorption, Refractive Index Changes, and All-Optical Switching. *Adv. Mater.* **2006**, 18, 1267-1270.

22. Menezes, J. W.; Ferreira, J.; Santos, M. J. L.; Cescato, L.; Brolo, A. G. Large-Area Fabrication of Periodic Arrays of Nanoholes in Metal Films and Their Application in Biosensing and Plasmonic-Enhanced Photovoltaics. *Adv. Funct. Mater.* **2010**, 20, 3918-3924.

23. van Beijnum, F.; Retif, C.; Smiet, C. B.; Liu, H.; Lalanne, P.; van Exter, M. P. Quasi-Cylindrical Wave Contribution in Experiments on Extraordinary Optical Transmission. *Nature* **2012**, 492, 411-414.

24. Li, Z.; Clark, A. W.; Cooper, J. M. Annular Nanoplasmonic Void Arrays as Tunable Surface Enhanced Raman Spectroscopy Substrates. *Appl. Phys. Lett.* **2014**, 105, 033115.

25. Genet, C.; Ebbesen, T. W. Light in Tiny Holes. *Nature* 2007, 445, 39-46.

26. Garcia-Vidal, F. J.; Martin-Moreno, L.; Ebbesen, T. W.; Kuipers, L. Light Passing through Subwavelength Apertures. *Rev. Mod. Phys.* **2010**, 82, 729-787.

27. Cheng, F.; Gao, J.; Luk, T. S.; Yang, X. D. Structural Color Printing Based on Plasmonic Metasurfaces of Perfect Light Absorption. *Sci. Rep.* **2015**, 5, 11045.

28. Alfalou, A.; Brosseau, C. Dual Encryption Scheme of Images Using Polarized Light. *Opt. Lett.* **2010**, 35, 2185-2187.

29. Tyo, J. S.; Goldstein, D. L.; Chenault, D. B.; Shaw, J. A. Review of Passive Imaging Polarimetry for Remote Sensing Applications. *Appl. Opt.* **2006**, 45, 5453-5469.

30. Laux, E.; Genet, C.; Skauli, T.; Ebbesen, T. W. Plasmonic Photon Sorters for Spectral and Polarimetric Imaging. *Nat. Photonics* **2008**, 2, 161-164.

31. Xie, Y.; Zakharian, A. R.; Moloney, J. V.; Mansuripur, M. Transmission of Light through Slit Apertures in Metallic Films. *Opt. Express* **2004**, 12, 6106-6121.

32. Silveirinha, M.; Belov, P.; Simovski, C. Subwavelength Imaging at Infrared Frequencies Using an Array of Metallic Nanorods. *Phys. Rev. B* **2007**, 75, 035108.

33. Chen, Q.; Das, D.; Chitnis, D.; Walls, K.; Drysdale, T. D.; Collins, S.; Cumming, D. R. S. A Cmos Image Sensor Integrated with Plasmonic Colour Filters. *Plasmonics* **2012**, 7, 695-699.

34. Zheng, B. Y.; Wang, Y. M.; Nordlander, P.; Halas, N. J. Color-Selective and Cmos-Compatible Photodetection Based on Aluminum Plasmonics. *Adv. Mater.* **2014**, 26, 6318-6323.

35. Darr, C. M.; Korampally, V.; Chen, B.; Gangopadhyay, K.; Gangopadhyay, S. Plasmonic-Enhanced Conjugated Polymer Fluorescence Chemosensor for Trace Nitroaromatic Vapor. *Sens. Actuators*, *B* **2014**, 202, 1088-1096.

36. Palik, E. D. *Handbook of Optical Constants of Solids.* Academic press: San Diego 1998.

TOC graphic: